Study on contribution of the asymmetric stress to the birefringence induced by an ultrashort single laser pulse inside fused silica glass

Somayeh Najafi, Reza Massudi, Aliasghar Ajami, Chandra S. R. Nathala, Wolfgang Husinsky, and Atoosa Sadat Arabanian

Citation: Journal of Applied Physics **120**, 153102 (2016); doi: 10.1063/1.4964870
View online: http://dx.doi.org/10.1063/1.4964870
View Table of Contents: http://scitation.aip.org/content/aip/journal/jap/120/15?ver=pdfcov
Published by the AIP Publishing

Study on contribution of the asymmetric stress to the birefringence induced by an ultrashort single laser pulse inside fused silica glass

Somayeh Najafi,[1] Reza Massudi,[1] Aliasghar Ajami,[2,3] Chandra S. R. Nathala,[2,4] Wolfgang Husinsky,[2] and Atoosa Sadat Arabanian[1,a)]
[1]*Laser and Plasma Research Institute, Shahid Beheshti University, G.C., Evin, Tehran, Iran*
[2]*Institute of Applied Physics, Vienna University of Technology, Wiedner Hauptstrasse. 8, 1060 Vienna, Austria*
[3]*Faculty of Physics, Semnan University, Semnan, Iran*
[4]*Femtolasers Productions GmbH, Fernkorngasse10, 1100 Vienna, Austria*

(Received 30 June 2016; accepted 2 October 2016; published online 18 October 2016)

Stress induced birefringence due to asymmetry in axial and radial directions that is generated because of the interaction of ultrashort laser pulses with a transparent material is numerically studied. The coupled equations of nonlinear Schrodinger and plasma density evolution are solved to calculate the deposited energy density and initial temperature profile. Fourier's heat equation and the equations related to the thermo-elasto plastic model are solved to calculate the temperature evolution and distribution of induced displacement inside the material, respectively. Finally, by numerically calculating the distribution of the induced refractive index changes experienced by both axially and radially probe beams, induced stress birefringence is calculated for different characteristics of writing pulses. Furthermore, the induced stress birefringence is experimentally realized, and the effect of the energy of the writing pulse is investigated. To know how the induced refractive index changes and birefringence distributions depend on parameters of the writing pulse is crucial to obtain high performance guiding structures and polarization-sensitive as well as polarization-independent components. *Published by AIP Publishing.*
[http://dx.doi.org/10.1063/1.4964870]

I. INTRODUCTION

The refractive index changes in a transparent material induced by ultrashort laser pulses have opened up prospects of producing three-dimensional integrated optical circuits in a single writing step.[1,2] These changes occur by the nonlinear absorption of the ultrashort laser pulse focused in the transparent material and, then, the creation of a hot zone near the focal point. Because of the wide range of transparency, from UV to IR, and the possibility of easy preparation of the high-quality substrates, fused silica glass is one of the most important materials to fabricate various optical waveguide devices including directional couplers,[3] Bragg grating waveguides,[4] waveguides in active materials,[5] and integrated lasers.[6] Furthermore, the capability to induce optical birefringence in the glass by ultrashort laser pulses has significantly developed the fabrication of integrated optics devices and provided a way to control the polarization of light propagating in the optical waveguides.[7]

Birefringence degree, defined as the difference between the effective refractive indices of the two polarization eigenmodes, in waveguides and optical fibers is an important issue in the design of optical circuits and fiber devices. A larger value of the birefringence can reduce the size of polarization-sensitive devices, such as waveplates,[8] polarizers, and polarization dependent directional couplers.[9] On the other hand, in some applications, lower birefringence is desired to minimize polarization mode dispersion in order to enable high speed optical data transmission[10] and to decrease the decoherence of polarization-entangled photon pairs in quantum optics applications.[11]

The fundamental mechanisms, which create the birefringence in the glass by femtosecond laser irradiation, are not still fully understood.[7] Fernandes *et al.* reported two major sources of the birefringence in waveguides fabricated by femtosecond laser exposure as form birefringence and anisotropic material stress. The former is related to laser induced nanogratings, which cause asymmetry in the (x,y)-plane. The latter is associated with inducing asymmetric stress with femtosecond laser fabricated modification tracks formed parallel to the waveguide axis.[12] Experimental verification of induced birefringence due to self-organized nanogratings has illustrated that the amount of birefringence depends on the pulse energy level, number of pulses, and their polarization direction.[7,10,13–15] Also, it has been proven that induced periodic nanostructures are aligned perpendicular to the polarization direction of the writing laser.[11] On the other hand, the angle between the direction of the polarization of the writing pulse and the waveguide axis is an effective factor on the induced birefringence degree, so that the amount of birefringence of waveguide written inside silica glass may vary from $\sim 10^{-6}$ to 4.35×10^{-4} by changing that angle.[12] It has also experimentally been observed that when the polarization of the writing beam is parallel with the waveguide direction, the amount of the induced birefringence is much smaller than when it is perpendicular to the waveguide direction.[10] That is probably because for the former configuration, the self-organized periodic nanostructures are aligned perpendicular

a)a_arabanian@sbu.ac.ir

to the waveguide direction and, therefore, the induced form birefringence is not experienced by the light coupled into the waveguide. Furthermore, when the writing process is performed by using a few number of pulses (below100 pulses), the induced nanogratings are not observed, and, hence, they do not contribute in the induced birefringence.

Although asymmetric stress birefringence can be generated by using adjacent tracks formed parallel to the waveguides,[12] Carrot- like geometry of energy distribution deposited by the single ultrashort pulse in the (r,z)-plane can also induce asymmetric stress birefringence in the focal region, which plays an important role when writing by using a few number of pulses. Anisotropic stress is a result of asymmetry of the deposited energy distribution in the axial and the radial directions during the interaction of ultrashort laser pulses with the material, which generates different refractive index changes in these directions (i.e., stress birefringence). Theoretical investigation of this type of birefringence is important due to its effect in waveguides, its potential application in the fabrication of polarization-dependent components, its role in generation of the nanostructures, and because of importance of eliminating the stress birefringence in manufacturing polarization-independent components. Different groups numerically studied laser-induced stresses, corresponding material relocation inside fused silica glass, which is asymmetric in radial and axial directions, and material density changes by using the volumetric strain.[16–18] However, to calculate the stress birefringence and its dependency on the processing parameters, the induced refractive index changes in two radial and axial directions should be calculated.

In this paper, we focus on the dependency of stress birefringence on incident pulse energy and duration, by numerically calculating the spatial distribution of the induced refractive index changes inside the transparent material. We apply a full strain-optic tensor to obtain induced refractive index changes,[19] which let us to compute the anisotropy of refractive index changes. We illustrate various distributions of refractive index changes experienced by two orthogonal polarizations of the probe light. It is observed that pulse parameters significantly affect the induced birefringence profile inside the material. Moreover, the calculation reveals that the largest negative and positive refractive index changes occur for, respectively, the axial polarization (AP) and radial polarization (RP) of the probe beam. Finally, the existence of stress birefringence and the effect of pulse energy in modified regions inside fused silica, which is illuminated by single shot laser pulse, are experimentally realized.

II. THEORY

Laser induced changes inside transparent materials include a complex chain of different processes, which sequentially occur at certain time intervals and eventually lead to permanent modifications inside the bulk of the material. The chain of processes occurring in the interaction of a focused ultrashort laser pulse with a transparent material is initiated with nonlinear absorption of ultrashort pulses inside the material. For pulses with the peak power higher than the critical power, $P_{cr} = \lambda^2/(2\pi n_0 n_2)$, the self-focusing effect increases the pulse intensity and, then, multiphoton ionisation (MPI) in the focal region. Therefore, the linear focusing and the self-focusing cause the excitation of electrons from the valence to the conduction bands. Consequently, the excited electrons can be further accelerated and their energies are increased by the electric field of the remaining part of the pulse. Energetic electrons excite other molecules or atoms by impact ionization and, then, repeating this procedure, an avalanche of high-energy electrons will be created. The effects of linear focusing, self-focusing, and plasma defocusing determine the distribution of the pulse intensity and the plasma density in the vicinity of the focus.[19] Then, the recombination of the electron–hole transfers energy from the excited electrons to the lattice within a few picoseconds and, consequently, the temperature of the nonlinear focal region quickly rises up and leads to softening. Rapid heating of the focal zone and the high thermal gradient of this region, relative to its surroundings, lead to stress, fast thermal expansion, and spreading of the heat pressure wave outward from the focal region. The carrot-like geometry of energy distribution deposited causes asymmetric stress and expansion and, hence, different heat pressure waves in radial and axial directions. The pressure wave displaces the material outside of the hot zone and, hence, the refractive index in that region reduces. On the other hand, the surrounding cold material prevents further spreading of the pressure wave and creates a weak compressive wave in the focal region, which is responsible for local densification and the increase of the refractive index around the irradiated region.[19] Asymmetric stress and heat pressure waves lead to different refractive index changes in radial and axial directions.

In this paper, by numerically solving the coupled equations of nonlinear Schrodinger (NLS) and plasma density evolution with employing the split step finite difference method (FDM), combined with alternating direction implicit (ADI) algorithm, the spatio-temporal distributions of the electric field envelop and the plasma density are calculated.[19] Those distributions are used to calculate the spatial distribution of the energy density deposited in the focal region, which is the energy distribution of the localized hot electrons in that region. Due to recombination of the electron- hole, the energy of the excited electrons is transferred to the lattice within a few picoseconds and, consequently, the temperature of the nonlinear focal region quickly rises up. Such spatio-temporal distribution of the hot zone temperature is achieved by using the classical Fourier's heat conduction theory and by numerically solving the Fourier equation using the hybrid Finite-Element Method (FEM)/Finite-Difference Method (FDM).[19]

A high thermal gradient of the hot zone relative to its surrounding leads to fast thermal expansion and displacement in the material where the components of the displacement vector are achieved by using following equations:

$$\rho\frac{\partial^2 u}{\partial t^2} = (2\mu+\lambda)\left[\frac{\partial^2 u}{\partial r^2}+\frac{1}{r}\frac{\partial u}{\partial r}-\frac{u}{r^2}\right]+\mu\frac{\partial^2 u}{\partial z^2} + (\mu+\lambda)\frac{\partial^2 w}{\partial z\partial r}-\beta\frac{\partial(T-T_0)}{\partial r}, \quad (1)$$

$$\rho\frac{\partial^2 w}{\partial t^2} = (2\mu+\lambda)\frac{\partial^2 w}{\partial z^2} + \mu\left[\frac{\partial^2 w}{\partial r^2} + \frac{1}{r}\frac{\partial w}{\partial r}\right] + (\mu+\lambda)\left[\frac{\partial^2 u}{\partial z \partial r} + \frac{1}{r}\frac{\partial u}{\partial z}\right] - \beta\frac{\partial (T-T_0)}{\partial z}, \quad (2)$$

where u and w are the radial and the axial components of the displacement vector, respectively, T_0 is the initial temperature, T(r,z,t) is the instantaneous temperature distribution in the focal region, and $\beta = (3\lambda + 2\mu)\alpha$, where α is the thermal expansion coefficient and $\mu = E_Y/2(1+\nu)$, and $\lambda = \nu E_Y/(1+\nu)(1-2\nu)$ are Lame constants, and E_Y and ν are Young's modulus and Poisson's ratio, respectively.

By replacing the temperature distribution calculated from Fourier equation and by numerically solving the coupled Equations (1) and (2), by using the FEM, the spatio-temporal distribution of displacement in the focal region and its surrounding is achieved. Next, one can calculate the components of the strain(ϵ) and the stress(σ) tensors.[19] To determine the regions with permanent modifications, the von-Mises criterion is verified. According to this criterion, if the value of the distortion energy per unit volume becomes higher than the energy per unit volume required to cause yield, the induced structural modification will be permanent.[21]

Any deformation of the optical material (ϵ_{kl}) modifies the index ellipsoid. Such modification changes B_{ij} tensor by the amount of ΔB_{ij} that for an optically isotropic material is related to the deformation ϵ_{kl} as[22]

$$\Delta B_{ij} = P_{ijkl}\epsilon_{kl}, \quad (3)$$

where P_{ijkl} is the elasto-optic tensor of the material. Then, by using Eq. (4), the refractive index changes of the material for probe light with radial (RP) and axial polarizations (AP) are calculated

$$\Delta n_{RP} = -\frac{1}{2}n_0^3 \Delta B_{rr},$$
$$\Delta n_{AP} = -\frac{1}{2}n_0^3 \Delta B_{zz}. \quad (4)$$

Finally, the induced birefringence distribution is calculated as

$$\delta = \Delta n_{AP} - \Delta n_{RP}. \quad (5)$$

By appropriate adjustment of the incident pulse parameters, the thermal profile in the focal region can be controlled. Asymmetric thermal distribution and, hence, different thermal gradients in the radial and the axial directions cause different stresses. Accordingly, the amount of displacements in the two directions (u, w in Eqs. (1) and (2)) is different, which causes asymmetric induced modification inside the material. Therefore, it is expected that the distribution of the induced refractive index changes that are experienced by probe lights with axial polarization (AP) and its perpendicular polarization (RP) to be different from each other, and, consequently, the amorphous glass presents birefringence after interaction with an ultrashort pulse.

III. RESULTS AND DISCUSSION

To investigate the induced stress birefringence inside the material, first, nonlinear equations describing propagation of an ultrashort laser pulse are numerically solved. Then, by calculating the absorbed energy of the pulse and using the equation of Fourier's heat conduction, evolution of temperature distribution is obtained. Next, the components of the displacement vector are calculated by using Eqs. (1) and (2) with the FEM. Finally, the profile of the refractive index changes for different polarizations of probe light and, consequently, the induced stress birefringence distribution are obtained by using Eq. (4). To determine the regions with permanent modifications, the von-Mises criterion is verified.

Let us assume a single laser pulse with a wavelength of 800 nm, and Gaussian temporal and spatial profiles are focused at the depth of 75 μm below the surface of a fused silica sample by a microscope objective with the magnification of 20× (NA = 0.5). The curvature of the wave and the beam waist at the entrance of the sample are assumed to be $R = 75.4\ \mu m$ and $W_0 = 13.19\ \mu m$, respectively (Fig. 1(a)). The parameters and physical constants used in this study are listed in Table I.

Nonlinear propagation of such a pulse inside the transparent material determines the spatial distribution of the deposited energy and the temperature profile in the focal region. Figs. 1(b)–1(d), respectively, show the temperature distribution due to the deposited energy inside the bulk of glass and the spatial distribution of the induced stress in radial (σ_{rr}) and axial (σ_{zz}) directions for a pulse with a duration of 100 fs (FWHM) and an energy of 1 μJ.

By comparing Figs. 1(c) and 1(d), one can see that the amplitude of the radial stress component is about 5 times larger than its corresponding axial one. Such behavior is because of the larger gradient of the deposited energy distribution in the radial direction as compared to the axial direction. Fig. 2 illustrates the profile of refractive index changes experienced by AP and RP probe beams induced by the writing pulse used in Fig. 1.

The figure illustrates that the reduction of the refractive index at the center of the hot zone is 30% larger for AP as compared to that of RP. Furthermore, it shows a small increase of refractive index at the edge of the hot zone for RP while such an increase is negligible for AP (Fig. 2(c)). The reason of such difference in refractive index distribution, which is experienced by AP and RP probe beams, is related to the asymmetry of the temperature profiles generated by ultrashort laser pulse in the axial and the radial directions. Since the Rayleigh range of the writing laser pulse propagating through the material is much longer than its focal spot size, the hot zone diameter in the axial direction (z) is longer than the radial direction. Thus, the molecules have more freedom of movement in the z-direction than in the radial direction, which results in further reduction of the refractive index for AP as compared to RP. On the other hand, the larger thermal gradient in the radial direction (located in plane x-y in Fig. 1) results in larger compression of the material in that direction and, consequently, a larger increase of the refractive index at the edges of the hot zone for RP.

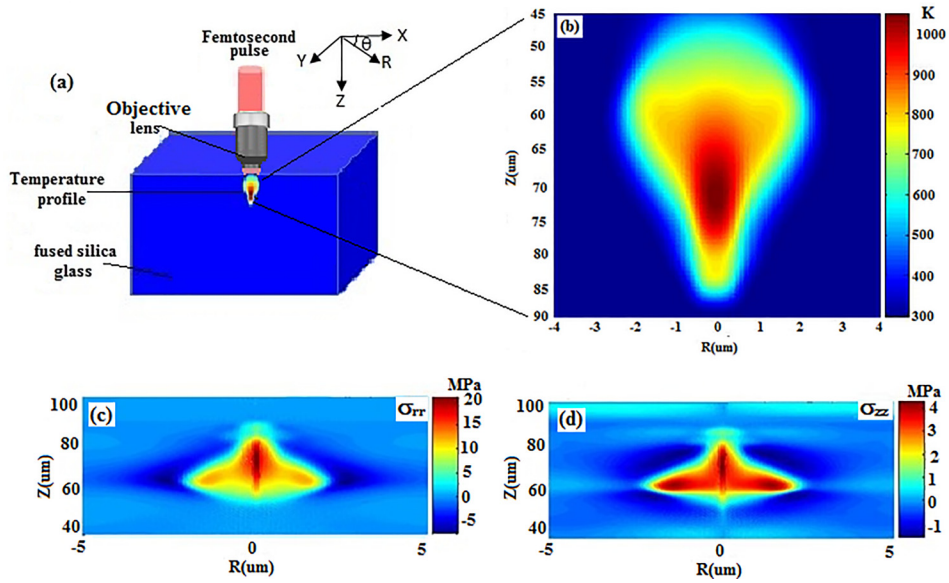

FIG. 1. (a) Schematic layout under study. Spatial distribution of (b) temperature, (c) radial stress component (σ_{rr}), and (d) axial stress component (σ_{zz}) induced by a pulse with an energy of 1 μJ and a duration of 100 fs.

TABLE I. Physical constants of fused silica glass.[20]

Linear refractive index (n_0)	1.45	Nonlinear refractive index (n_2)	3.54×10^{-16} (cm^2/w)
Band gap energy (E_g)	9 (eV)	Inverse bremsstrahlung cross section (σ_{br})	$1.55 \times 10{-}18$ (cm^2)
Cross section of the MPI (σ_6)	9.8×10^{-70} (cm^{12}/(s.w^6))	Coefficient of group velocity dispersion (k'')	361 (fs^2/cm)
Critical electron density (ρ_{BD})	1.74×10^{21} (cm^{-3})	Relaxation time (τ_{tr})	150 (fs)
Specific heat capacity (C_p)	703 (J/(kg K))	Volumetric heat capacity (C_{lat})	1.7 (J/(cm^3 K))
Thermal expansion coefficient (α)	55×10^{-8} (1/K)	Poisson's ratio (ν)	0.17
Young's modulus (E_y)	73.1 (GPa)	Elasto-optic coefficient	$P_{11} = 0.121$, $P_{12} = 0.270$, $P_{44} = -0.0745$
Power critical	1 .98 MW		

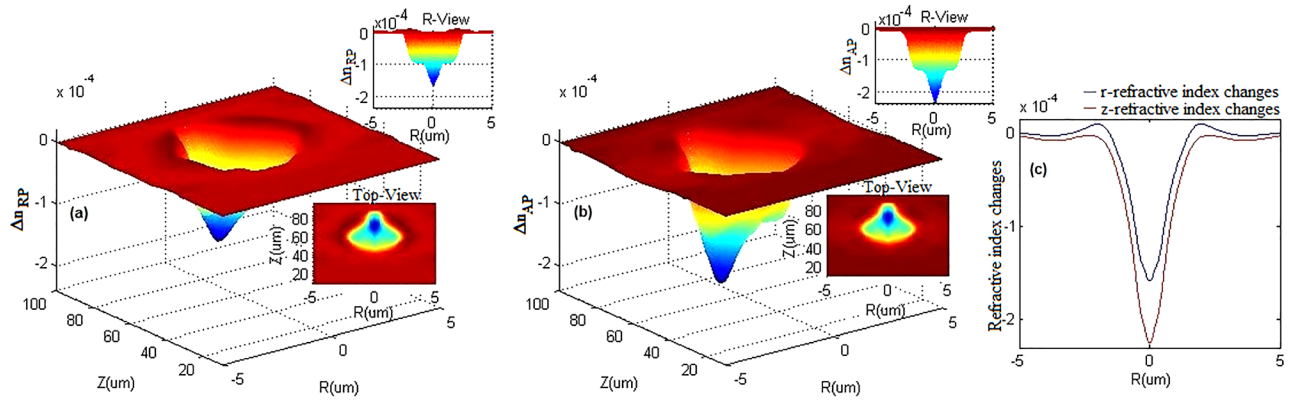

FIG. 2. The profile of the refractive index changes for (a) RP and (b) AP probe beams induced by a pulse with an energy of 1 μJ and a duration of 100 fs. (c) Refractive index changes experienced by the two probe polarizations at a depth of 75 μm.

For more clarification, one can verify that a symmetric thermal profile in axial and radial directions creates a refractive index profile that is identical for both probe light polarizations. Fig. 3 illustrates the spatial profile of the refractive index changes induced by the Gaussian thermal profile and experienced by an RP beam. Here, the temperature peak is assumed similar to that of Fig. 1(b) (~1044 K) and its waist equal to the average radius of that profile (~6.5 μm). Similar behavior is observed for the AP probe beam.

In the following, we study on dependence of the stress-induced birefringence profile on different parameters of the incident pulse. Fig. 4 illustrates the distribution of the refractive index changes for different peak powers of the writing pulses with durations ranging from 200 fs to 50 fs and an energy of 1 μJ. One can see that for the pulse with a duration of 200 fs, the maximum refractive index changes occur at the center of the profile and are -1.52×10^{-4} for RP and -2.15×10^{-4} for AP probe beams (Figs. 4(a1) and 4(b1)). The corresponding values for a 50 fs pulse are -1.91×10^{-4} and -2.63×10^{-4}, respectively (Figs. 4(a2) and 4(b2)). In the other words, increasing the peak power from 5 MW to 20 MW, by reducing the pulse duration from 200 fs to 50 fs,

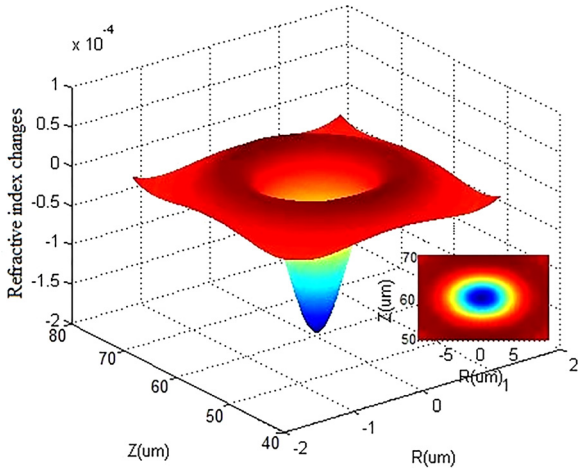

FIG. 3. Spatial distribution of the refractive index change generated by a Gaussian thermal profile with a peak temperature of 1044 K.

increases the maximum corresponding birefringence from 6.3×10^{-5} (in Fig. 5(c1)) to 7.2×10^{-5} (in Fig. 4(c2)).

The effect of increasing the peak power by adding the energy of the writing pulse from 1 μJ to 3 μJ for a pulse duration of 400 fs on the induced refractive index profile that is experienced by RP and AP probe beams is shown in Fig. 5. Although, the peak power of the writing pulse for Fig. 5(a2) is about 37% of that in Fig. 4(a2), regions with large negative refractive index changes ($\Delta n < 0$), in addition to the nonlinear focus area, are also created in larger radii closer to the surface (top view in Fig. 5(a2)). Such behavior is due to the higher deposited energy and generated electron density and, thus, much greater defocusing effect on the trailing part of the writing pulse. Therefore, the regions with negative refractive index changes in Fig. 5(a2) appear in cone-shaped. The difference of negative refractive index changes experienced at the tip and off axis regions of the cone by AP probe beam is about 70% larger than that of the RP probe beam (R-view in Fig. 5). For a pulse with an energy of 1 μJ, the largest amount of refractive index changes occurs on the tip of the cone, which is -1.23×10^{-4} for RP and -1.7×10^{-4} for AP probe beams (Figs. 5(a1) and 5(b1)), whereas the corresponding values for an energy of 3 μJ are -1.37×10^{-4} and -1.92×10^{-4}, respectively (Figs. 5(a2) and 5(b2)). Therefore, the peak value of the birefringence distribution increases from 5.0×10^{-5} for the energy of 1 μJ to 5.6×10^{-5} for the writing pulse with the energy of 3 μJ.

On the other hand, heat accumulation of multipulse has an important role in induced modification inside the material when using a high repetition rate system (about tens of MHz). That is because cooling of the hot zone inside the fused silica glass lasts a few microseconds. Therefore, heat accumulation occurs for pulse train with the time interval of less than 1 μs. To study the heat accumulation effect, induced refractive index changes inside fused silica are compared for two different conditions of irradiation, which induce a similar temperature peak of 1100 K, namely, irradiation by a single pulse with an energy of 1 μJ, a pulse duration of 50 fs, and a high peak power of 20 MW; and irradiation by successive three pulses under heat accumulation conditions, an energy per pulse of 1 μJ, a pulse duration of 1 ps, and a low peak power of 1 MW. The largest refractive index change for single pulse writing occurs at the depth of 71.5 μm and is -2.63×10^{-4} for AP and -1.91×10^{-4} for RP probe beams (Figs. 4(a2)–4(c2)). The corresponding condition for three pulses writing occurs at the depth of 73 μm where the largest values of refractive index changes are -2.5×10^{-4} and -1.8×10^{-4} for AP and RP beams, respectively (Figs. 6(a)–6(c)). Therefore, although the maximum value of the induced birefringence is the same for both configurations, the modified region is more localized and more symmetry for three pulses configuration with low peak power as compared to high peak power single pulse irradiation.

The results obtained so far suggest the possibility of designing polarization dependent components by adjusting the pulse characteristics. Furthermore, irradiating the sample by adjacent pulses with appropriate distances from each other can increase design capability. By using two pulses,

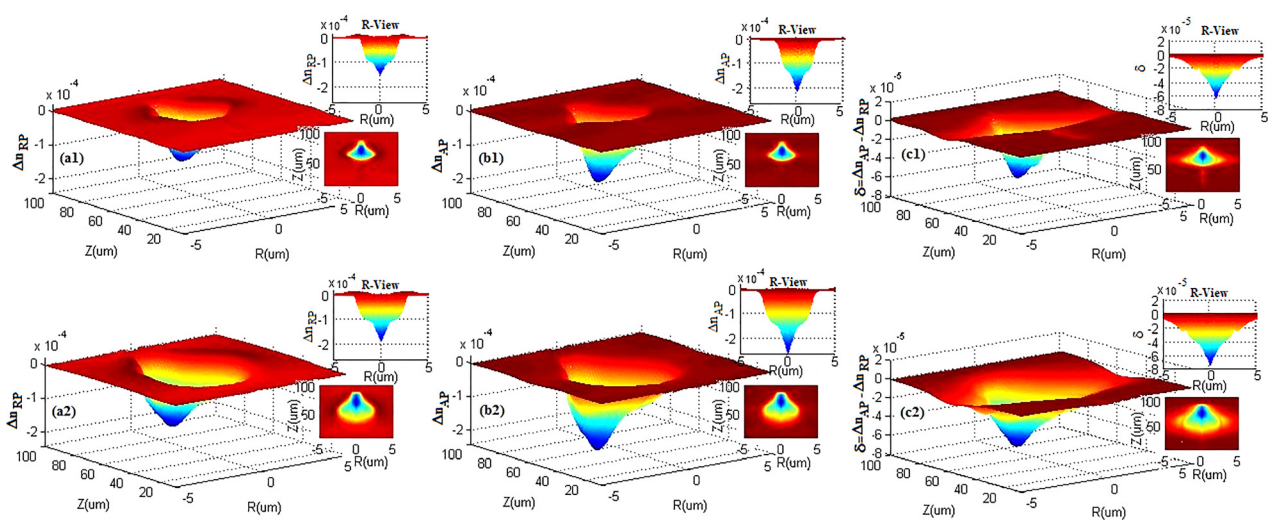

FIG. 4. Spatial distribution of the refractive index changes experienced by RP (a1) and (a2), AP probe beams (b1) and (b2), and spatial profile of birefringence (c1) and (c2) induced by an ultrashort laser pulse with an energy of 1 μJ and durations of 200 fs (a1)–(c1) and 50 fs (a2)–(c2).

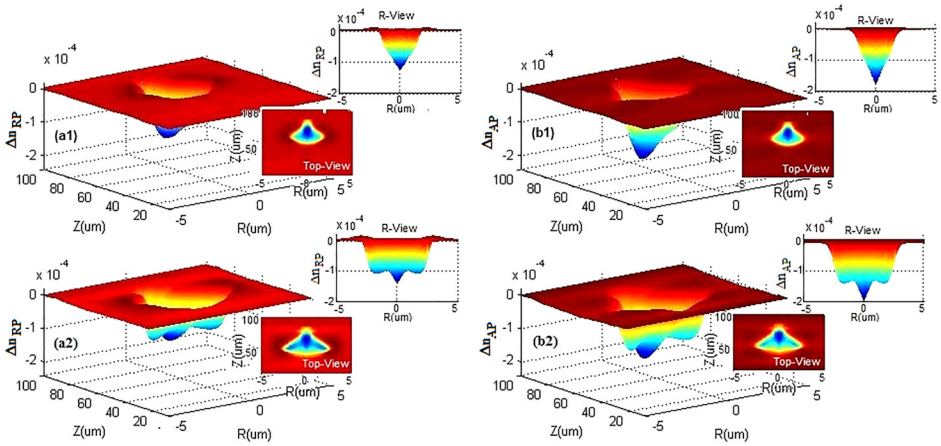

FIG. 5. Spatial distribution of the refractive index changes for RP (a1), (a2) and AP probe beams (b1), (b2) induced by an ultrashort writing pulse with a duration of 400 fs and energies of 1 μJ (a1) and (b1) and 3 μJ (a2) and (b2).

which are appropriately separated in the x-direction, the symmetry in the x-y plane can be broken to induce birefringence in this plane. Fig. 7(a) shows the region with positive refractive index changes for the RP probe beam (i.e., polarization vector in plane x-y) induced by the writing pulse used in Fig. 4(a2). Variation of such changes vs. radius at a depth of 60 μm is shown in Fig. 7(b) where the area with positive Δn_{RP} is specified by arrows. Irradiating the sample with another similar pulse at the distance of 5 μm from the former pulse, the region with positive refractive index changes (specified by an arrow in Fig. 7(c)) is surrounded between two regions with large negative refractive index changes in the x-direction, while such behavior is not observed in the y-direction. That results in induced birefringence in the x-y plane.

To experimentally realize the existence of induced stress birefringence, Ti:sapphire laser pulses at the wavelength of 800 nm, duration of 200 fs, repetition rate of 1 kHz, and energy ranging between 1 and 3 μJ (Femtolasers, Inc.) are focused at the depth of 100 μm inside fused silica glass by using a 50× microscope objective (NA = 0.65). The sample is moved with a speed of 1 cm/s by using an XYZ-Stage (ABL 10150 Air Bearing Stage, Aerotech, Inc.). Such movement separates the irradiated area by each shot by distances of 10 μm from each other. Figs. 8(a1)–8(c1) show the phase contrast microscopy (Olympus BX-51) images of the modified regions by single shots with the energies of (a1) 1 μJ, (b1) 2 μJ, and (c1) 3 μJ when the surface of the sample is adjusted perpendicular to the axis of the microscope. In a positive phase contrast microscopy (PCM) image, the white/dark color indicates the refractive index decrease/increase. We observe that the refractive index changes at the center of modified regions are negative that confirm the validity of our numerical results.

To investigate the birefringence induced by single shots inside fused silica, the sample is also placed between two orthogonal polarizers in a polarization microscope (Nikon, Optiphot2-Pol). Since the periodic nano-structures can only be observed when the number of applied shots are more than 100 pulses,[13] therefore, in the present images, only asymmetric stresses contributes on generation of induced birefringence.

As described in the numerical part, such stress birefringence for the modified region in the location of single shot is due to the asymmetric thermal profile in the axial (z) and radial (x-y plane) directions. To study the birefringence induced inside fused silica, our experiments are carried out in the following two situations. When the surface of the sample is adjusted perpendicular to the axis of the microscope, the polarization vector of the probe light is in the x-y plane of the sample. Hence, it does not have a component in the axial direction and the asymmetric stress birefringence is not detected. Figs. 8(a2)–8(c2) show the images of polarization microscopy of the sample for the writing pulse with energies varying from 1 to 3 μJ. As shown in this figure, birefringence is not observed in the location irradiation. Little birefringence that appeared in the distance between two adjacent shots is due to elimination of the symmetry in the x-y plane, which was predicted by numerical results in Fig. 7(c). Furthermore, it is seen that the birefringence in the distances between two consequent shots decreases with reducing the energy of the writing pulse because of lower lateral-asymmetric stresses.

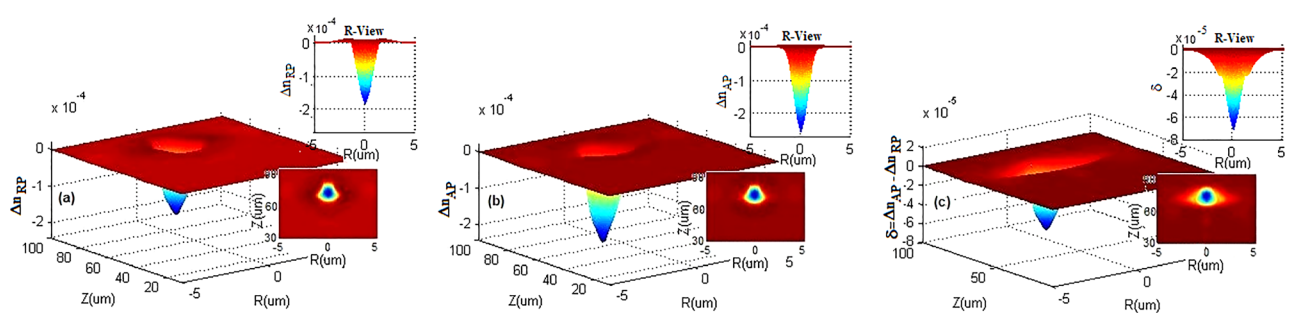

FIG. 6. Spatial distribution of the refractive index changes for RP (a), AP probe beams (b), and spatial profile of birefringence (c) induced by three ultrashort laser pulses with an energy per pulse of 1 μJ and a pulse duration of 1 ps.

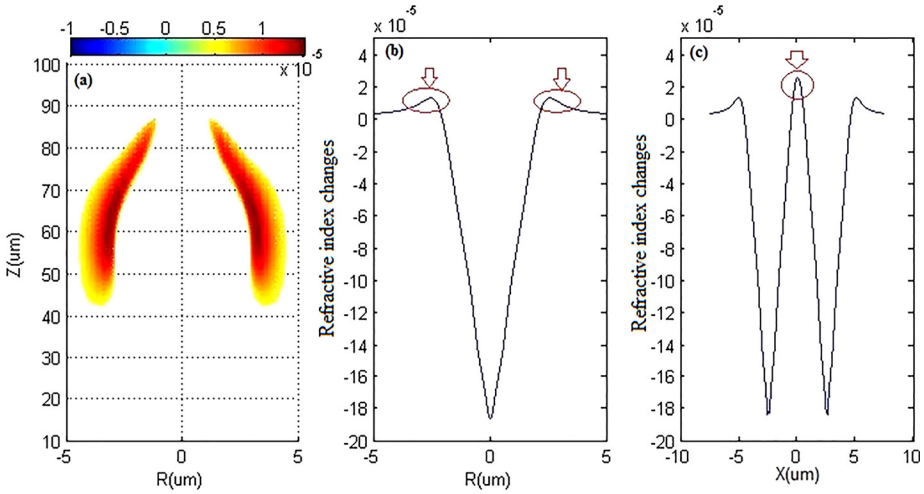

FIG. 7. (a) Spatial distribution of positive refractive index changes experienced by the RP probe beam (in Fig. 4(a2)), (b) variation of the refractive index changes at a depth of 60 μm, (c) overlap of the refractive index modifications at a depth of 60 μm induced by two similar pulses with a duration of 50 fs and an energy of 1 μJ, which are seperated by 5 μm in the x-direction.

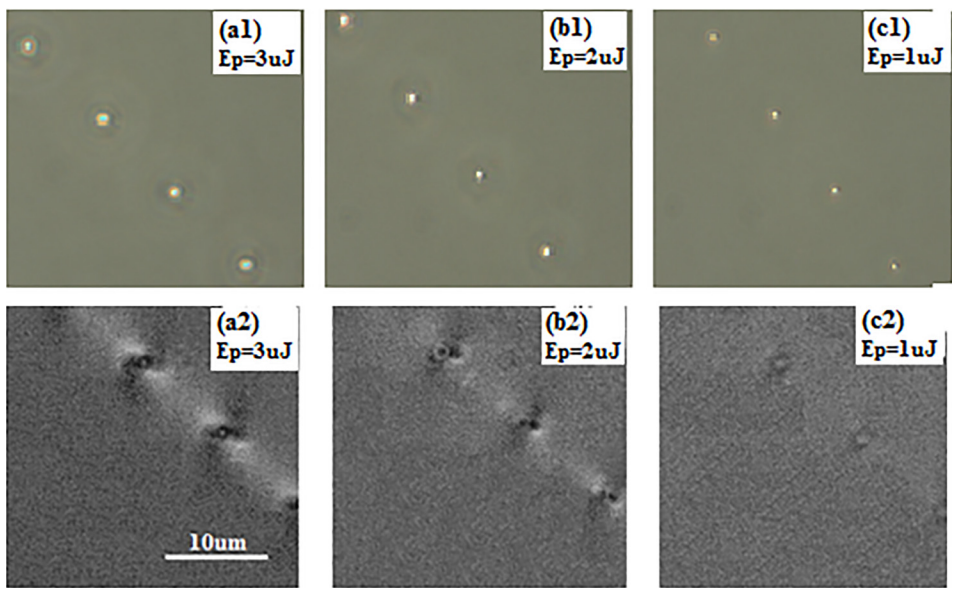

FIG. 8. PCM images of the modified regions by single shots with energies of (a1) 3 μJ, (b1) 2 μJ, and (c1) 1 μJ. Polarization microscopy images for the corresponding regions irradiated by single shots with energies of (a2) 3 μJ, (b2) 2 μJ, and (c2) 1 μJ.

In the second configuration, to observe the birefringence caused by asymmetric stress in axial and radial directions inside the material, the sample is tilted about 10° relative to the axis of the microscope so that the polarization vector of the probe light has a component along the z-axis of the sample. Fig. 9 shows the polarization microscopy images of the regions modified by single shots with energies of 1–3 μJ. Bright points that are observed in the irradiated area stand for the stress induced birefringence. Moreover, the figures illustrate that reducing the pulse energy leads to decrease of the stress birefringence.

IV. CONCLUSION

A comprehensive numerical study on stress birefringence induced by ultrashort laser pulses focused inside the fused silica was implemented. The coupled nonlinear Schrodinger equation and plasma density evolution equation

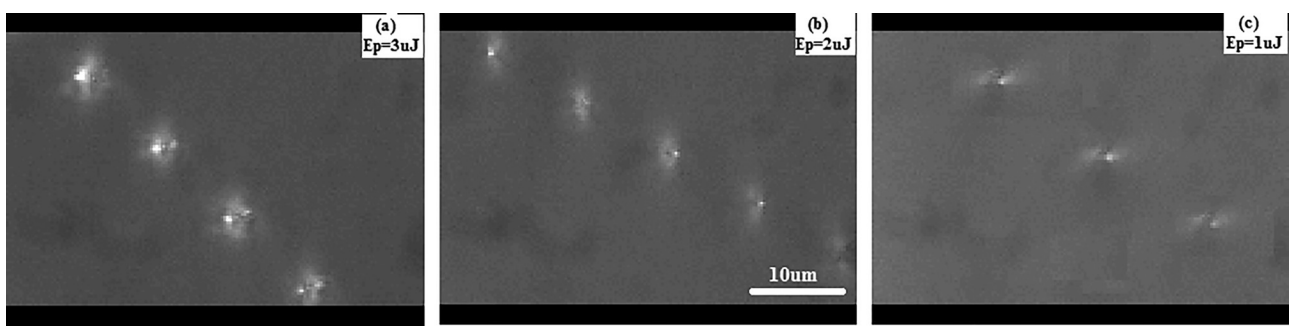

FIG. 9. Polarization microscopy images of fused silica irradiated by single shots with an energy of (a) 3 μJ, (b) 2 μJ, and (c) 1 μJ with an angle of about 10°.

were numerically solved to calculate the distribution of the deposited energy density of the writing pulse inside the transparent material and to obtain initial temperature distribution in the focal region. Then, temperature evolution of the material around the focal region was calculated by using classical Fourier's heat conduction theory and by numerically solving the Fourier equation with the hybrid FEM/FDM. Consequently, the distribution of induced displacement was obtained by using the thermo-elasto plastic model with the FEM. Finally, by numerical calculation of the distribution of induced refractive index changes for both AP and RP probe beams, induced stress birefringence was calculated. Furthermore, we investigated the dependency of such birefringence on writing pulse characteristics. It was shown that the pulse parameters significantly affect the distribution of induced stress birefringence. It was also observed when using three pulses with lower peak power, as compared to single pulse with higher peak power, the distribution of the induced stress- birefringence is more localized. Moreover, our calculations reveal that the largest negative and positive refractive index changes occur for AP and RP probe beams, respectively. Such results can be used to design polarization-sensitive as well as polarization-independent components. We also experimentally realized stress birefringence and showed the effect of energy of writing pulse on it.

[1]S. Nolte, M. Will, J. Burghoff, and A. Tuennermann, Appl. Phys. A **77**, 109–111 (2003).
[2]A. Kowalevicz, V. Sharma, E. Ippen, J. G. Fujimoto, and K. Minoshima, Opt. Lett. **30**(9), 1060–1062 (2005).
[3]S. M. Eaton, W.-J. Chen, H. Zhang, R. Iyer, J. Li, M. L. Ng, S. Ho, J. S. Aitchison, and P. R. Herman, J. Lightwave Technol. **27**(9), 1079–1085 (2009).
[4]H. Zhang, S. M. Eaton, and P. R. Herman, Opt. Lett. **32**(17), 2559–2561 (2007).
[5]R. Osellame, N. Chiodo, G. Della Valle, S. Taccheo, R. Ramponi, G. Cerullo, A. Killi, U. Morgner, M. Lederer, and D. Kopf, Opt. Lett. **29**(16), 1900–1902 (2004).
[6]M. Ams, P. Dekker, G. D. Marshall, and M. J. Withford, Opt. Lett. **34**(3), 247–249 (2009).
[7]P. Yang, G. R. Burns, J. Guo, T. S. Luk, and G. A. Vawter, J. Appl. Phys. **95**(10), 5280–5283 (2004).
[8]L. A. Fernandes, J. R. Grenier, P. R. Herman, J. S. Aitchison, and P. V. Marques, Opt. Express **19**(19), 18294–18301 (2011).
[9]L. A. Fernandes, J. R. Grenier, P. R. Herman, J. S. Aitchison, and P. V. Marques, Opt. Express **19**(13), 11992–11999 (2011).
[10]L. A. Fernandes, J. R. Grenier, P. V. Marques, J. Stewart Aitchison, and P. R. Herman, J. Lightwave Technol. **31**(22), 3563–3569 (2013).
[11]C. Antonelli, M. Shtaif, and M. Brodsky, Phys. Rev. Lett. **106**(8), 080404 (2011).
[12]L. A. Fernandes, J. R. Grenier, P. R. Herman, J. S. Aitchison, and P. V. Marques, Opt. Express **20**(22), 24103–24114 (2012).
[13]Y. Shimotsuma, M. Sakakura, P. G. Kazansky, M. Beresna, J. Qiu, K. Miura, and K. Hirao, Adv. Mater. **22**(36), 4039–4043 (2010).
[14]F. Zimmermann, A. Plech, S. Richter, A. Tünnermann, and S. Nolte, Proc. SPIE **9355**, 935512 (2015).
[15]M. Lancry, B. Poumellec, J. Canning, K. Cook, J. C. Poulin, and F. Brisset, Laser Photonics Rev. **7**(6), 953–962 (2013).
[16]N. M. Bulgakova, V. P. Zhukov, S. V. Sonina, and Y. P. Meshcheryakov, J. Appl. Phys. **118**(23), 233108 (2015).
[17]J. S. Petrovic, V. Mezentsev, H. Schmitz, and I. Bennion, Opt. Quantum Electron. **39**(10–11), 939–946 (2007).
[18]A. Mermillod-Blondin, I. M. Burakov, Y. P. Meshcheryakov, N. M. Bulgakova, E. Audouard, A. Rosenfeld, A. Husakou, I. V. Hertel, and R. Stoian, Phys. Rev. B **77**(10), 104205 (2008).
[19]S. Najafi, A. S. Arabanian, and R. Massudi, J. Phys. D: Appl. Phys. **49**(25), 255101 (2016).
[20]L. Sudrie, A. Couairon, M. Franco, B. Lamouroux, B. Prade, S. Tzortzakis, and A. Mysyrowicz, Phys. Rev. Lett. **89**(18), 186601 (2002).
[21]M. L. Wilkins, *Calculation of Elastic-Plastic Flow* (University of California, Livermore, CA, 1963).
[22]D. Royer and E. Dieulesaint, *Elastic Waves in Solids II: Generation, Acousto-Optic Interaction, Applications* (Springer Science & Business Media, 2000).